A-GNSS Sensitivity for Parallel Acquisition in Asynchronous Cellular Networks

Seung-Hyun Kong, *Member, IEEE,* and Wooseok Nam, *Member, IEEE*

***Abstract*—Increasing the dwell time in two-dimensional frequency-time hypothesis testing is, in practical terms, one of the most effective ways for Assisted Global Navigation Satellite Systems (A-GNSS) and GNSS receivers to achieve higher sensitivity. In an asynchronous cellular network, however, a mobile terminal may have a non-negligible unknown clock drift rate error originating from the received cellular downlink signal. In such a case, increasing the dwell time may not necessarily result in the expected sensitivity improvement. In addition, a mobile terminal in a rich multipath environment may experience jitters in the code phase of the resolved first arrival path due to short-delay multipaths, which also degrades the sensitivity. In this paper, new decision variables using a lone or a pair of adjacent H_1 cells for code phase hypothesis testing and clock drift rate hypothesis testing are proposed to cope with the unknown code phase drift rate error and the effect of code phase jitter in a parallel acquisition system. The statistics of the proposed decision variables are analyzed in a Rayleigh fading channel, and the performances of the proposed decision variables are compared with that of the conventional decision variable.**

***Index Terms*—Assisted GNSS, assisted GPS, parallel acquisition, asynchronous cellular networks.**

I. Introduction

THE Assisted Global Navigation Satellite System (A-GNSS) is one of the most popularly used mobile localization technologies to support the growing demand for location-based services. A-GNSS can achieve high sensitivity with assistance from cellular networks, as defined in [1] and [2]. An A-GNSS receiver performs two-dimensional frequency-time hypothesis testing, which can be simply implemented with a parallel acquisition system [3], [4]. In addition, the dwell time can be increased by the accumulation of multiple integration results. For example, the frequency uncertainty of the Global Positioning System (GPS) $L1$ carrier frequency (1.575GHz) due to the relative motion between a GPS receiver and a GPS satellite is typically within $[-6, 6]$kHz, and the code phase (time) uncertainty can be as large as the PRN code length (1023 chips) of the GPS $L1$ Coarse Acquisition (C/A) signal [5]. Typical two-dimensional frequency-time hypothesis testing consists of an outer loop for frequency searches with a step size of less than 500Hz, and an inner loop for code phase searches with a step size of half a chip, as in [5] and [6].

To increase the sensitivity in GNSS signal acquisition, an A-GNSS receiver in a synchronous cellular network, such as IS-95 and CDMA2000, is provided with an accurate code phase estimate with a few chips (microseconds) of uncertainty and other navigation information by the cellular network [1]. However, the code phase estimate provided to A-GNSS receivers by asynchronous cellular networks, such as the Global System for Mobile (GSM) and the Wideband Code Division Multiple Access (WCDMA) systems, has seconds of uncertainty when the networks do not have Location Measurement Unit (LMU) [2]. Consequently, the acquisition performance and the achievable sensitivity in asynchronous networks are poorer than those in synchronous networks. In addition, given that mobile terminals rely on the received downlink signal frequency and timing reference, non-negligible and time-varying clock drift can arise in the receiver-generated clock in asynchronous cellular networks. In practice, stringent carrier frequency and clock drift rate tolerance requirements for the IS-95 and CDMA2000 downlinks are well satisfied, as the base stations are equipped with fine GNSS receivers for the synchronization of all base stations. However, GSM and WCDMA do not have such stringent frequency and clock drift rate tolerance requirements for downlinks; GSM and WCDMA allow a maximum of ± 0.1ppm error in the downlink carrier frequency. Moreover, user terminals are required to maintain synchronization to the carrier frequency of the received downlink signal within ± 0.1ppm [7]-[9].

In many A-GNSS applications, indoor environments and deep urban canyons are the most challenging environments, as GNSS receivers in these type of areas usually experience very weak received signal strength. In such challenging environments, GNSS signals often arrive at the receiver via multiple Non-Line of Sight (NLOS) paths and therefore experience considerable path loss due to obstacles such as buildings. These multipaths cause fading in the signal amplitude and entail unknown pseudorange error as well. In [5], it was found that short-delay multipaths constituting a resolved first arrival path can lead to detection errors in code phase. The detected code phase error also varies according to the relative phase and delay between the dominant path and the short-delay multipaths. Intuitively, when only NLOS multipaths constitute the resolved path, the detected code phase can vary significantly as the delay and phase of each short-delay multipath vary randomly. This results in a time-varying code phase jitter that is not negligible for the GNSS signal acquisition system.

Many sensitivity improvement schemes for GNSS receivers introduced in the literature focus on mitigating the large time uncertainty. Recent studies show that GPS navigation bit transition and substantial frequency drift larger than half of the frequency search step size during the GPS signal search can be handled [10], [11]. In [12], joint Bayesian estimation of the time and frequency offsets for GPS is considered for improved

Manuscript received January 15, 2010; revised June 30, 2010 and September 3, 2010; accepted September 4, 2010. The associate editor coordinating the review of this paper and approving it for publication was G. Colavolpe.

The authors are with the Department of Aerospace Engineering, Korea Advanced Institute of Science and Technology, Daejeon, Korea (e-mail: skong@kaist.ac.kr, wsnam@stein.kaist.ac.kr).

Digital Object Identifier 10.1109/TWC.2010.092810.100070

sensitivity over conventional matched-filter-type receivers. In [13], a sensitivity improvement scheme using two adjacent H_1 (correct code phase hypothesis) cells is introduced for a serial acquisition system. The joint two H_1 cell-based detection approach makes use of the fact that there are two H_1 cells within a half chip from the correct code phase of a resolved path.

In this paper, single and joint two H_1 cell-based detection schemes are modified to propose decision variables for A-GNSS parallel acquisition in asynchronous cellular networks. The performances of the proposed decision variables are analyzed in a Rayleigh fading channel [14] as a general channel model for GPS in urban canyons and indoor environments. Though we focus on the GPS C/A signal, the arguments in this paper can directly be applied to any other GNSS spread spectrum signals.

The remainder of this paper is organized as follows. In Section II, we investigate the code phase jitters of GPS signals in urban environments to derive algebraic expressions of the baseband-equivalent GPS signal. Section III describes parallel acquisition systems and introduces the proposed decision variables to cope with the effects of an asynchronous cellular network. In Section IV, we derive algebraic expressions for the proposed detection variables in a parallel acquisition system. Section V provides algebraic and numerical performance analyses of a parallel acquisition system with the proposed detection variables. Particularly, the receiver operating characteristics (ROC) of the parallel acquisition system with the proposed decision variables are computed. Moreover, the code phase acquisition performances of the proposed schemes are numerically evaluated and compared to that of the conventional scheme. Finally, conclusions are provided in Section VI.

II. A-GPS in Urban Environments

As stated in [7] and [9], a mobile terminal in an asynchronous cellular network can have maximum oscillator drift of about ± 0.2ppm due to the frequency drift in the received signal that originates from the oscillator at the base station and the inaccuracy of the frequency tracking function. The oscillator drift of ± 0.2ppm can result in a frequency drift of ± 400Hz for a 2GHz carrier frequency, as well as a clock drift of ± 0.2 samples per second for a sampling clock with a 1MHz sampling rate. In practice, the oscillator of the mobile terminal is shared with an integrated A-GPS receiver [6], and we assume that the A-GPS receiver is performing parallel acquisition with $N_I (\gg 1)$ non-coherent matched filters (MF), as illustrated in Fig. 1. Let the $L1$ C/A signal transmitted by the kth GPS satellite at time t be expressed as

$$s_k(t) = \sqrt{2} b_k(t) c_k(t) \cos(2\pi f_{L1} t + \phi_{s,k}), \tag{1}$$

where $b_k(t)$, $c_k(t)$, f_{L1}, and $\phi_{s,k}$ represent the navigation bit of a 50bps baud rate, a spreading pseudorandom noise (PRN) code with a length of 1023 at a 1.023Mcps chip rate, the $L1$ carrier frequency, and an unknown carrier phase of the transmitted signal at time t, respectively. Let $L_R(t)$ and $L_{SV,k}(t)$ represent the receiver's location and the kth GPS satellite location, respectively, at time t in an Earth Centered

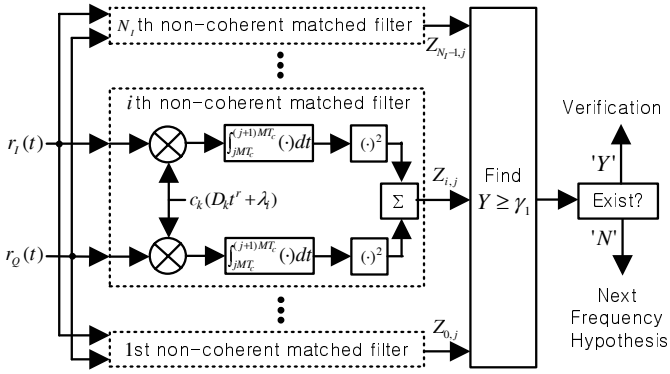

Fig. 1. Proposed parallel acquisition scheme.

Earth Fixed (ECEF) coordinate system, and let $t = t_i$ be the time when $s_k(t)$ arrives at the receiver after propagating τ_i seconds. The measured propagation delay $\tau(t)$ at t around t_i can then be expressed as

$$\tau(t) = \tau_i - \frac{V_k(t)}{c}(t - t_i) + \tau_m(t), \tag{2}$$

where $V_k(t)$ is the velocity component of the kth GPS satellite motion towards the receiver

$$V_k(t) = \frac{[L_R(t) - L_{SV,k}(t)]^T \cdot \frac{d}{dt} L_{SV,k}(t - \tau_i)}{\|L_R(t) - L_{SV,k}(t)\|}, \tag{3}$$

c is the speed of light, and $\tau_m(t)$ represents the code phase measurement error at time t due to the short-delay multipaths. Note that $V_k(t)$ (3) is usually slowly varying; we assume it is almost constant, i.e., $V_k(t) = V_k$, for the time duration of interest.

In practice, a resolved path in urban and indoor environments is often constructed by a number of short-delay multipaths [5] that arrive at the receiver no later than a chip after the LOS path. As there can be multiple scatterers at different locations around a receiver, each short-delay multipath can be assumed to have an independent random phase, so that the code phase of the resolved path has a time-varying measurement error $\tau_m(t)$ in (2). Moreover, when there are only one dominant path (typically LOS path) and one weak short-delay multipath with random phase relative to the dominant path, $\tau_m(t)$ has a distribution within a narrow range

$$\tau_m(t) \in [-\delta\tau, \delta\tau]. \tag{4}$$

In [5], it was shown that $\delta\tau$ (4) depends on the relative strength and relative delay between two paths when only two paths are present. In many urban canyon and indoor environments, the LOS path is severely attenuated due to obstacles, but there can be multiple dominant short-delay multipaths. Given that the number of short-delay multipaths as well as the relative phase and code phase of each dominant short-delay multipath can vary significantly during a long dwell time, $\delta\tau$ in (4) typically cannot be assumed to be very small; therefore, the variation of $\tau_m(t)$ is not negligible.

The autocorrelation function of the GPS C/A code, $R(t)$, is

expressed as

$$R(t) \simeq \begin{cases} 1-\dfrac{|t|}{T_c}, & |t|<T_c, \\ 0, & \text{otherwise.} \end{cases} \quad (5)$$

Denoting $T_c(=0.9775\mu s)$ as the chip length of the $L1$ C/A signal and $\tau_{s_l}(t)$ $(l=1,2,...L)$ as the code phases of short-delay multipaths at time t, the measured code phase from the correlation peak of the resolved path at time t is given by

$$\tau_m(t) = \arg\max_{\tau} \left| R(\tau) * \sum_{l=1}^{L} \beta_l(t)\delta(\tau-\tau_{s_l}(t))\exp(-j\psi_l(t)) \right|, \quad (6)$$

where '$*$' represents the convolution operation, and $\beta_l(t)$ and $\psi_l(t)$ are the amplitude and phase of the lth short-delay multipath $(l=1,2,...,L)$ at time t, respectively. Note that $\tau_m(t)$ depends on the distribution of $\beta_l(t)$, $\tau_{s_l}(t)$, and $\psi_l(t)$. Without loss of generality, the phase of each path $\psi_l(t)$ is uniformly distributed over $(-\pi,\pi]$. Regarding the amplitude of each path, we assume that the channel has dominant short-delay multipaths and severely attenuated LOS; thus, $\beta_m(t)/\beta_n(t)$, $(1 \le m,n \le L)$, is relatively small. At two different time instants t_i and t_{i+1}, the code phase jitter is defined as

$$\Delta\tau = \tau_m(t_{i+1})-\tau_m(t_i). \quad (7)$$

Assuming that t_i and t_{i+1} are sufficiently far apart such that we can assume $\tau_m(t_i)$ and $\tau_m(t_{i+1})$ to be statistically independent, Fig. 2 shows the empirical distributions of the code phase jitter obtained from 10^6 Monte Carlo trials for $0.5 \le \beta_m(t)/\beta_n(t) \le 1.5$, $(1 \le m,n \le L)$. For the distribution of $\tau_{s_l}(t)$, a uniform distribution $f^U_{\tau_s}(t)$ and an exponential distribution $f^E_{\tau_s}(t)$

$$f^U_{\tau_s}(t) = \frac{2}{T_c}\big[u(t)-u(t-\frac{T_c}{2})\big], \quad (8)$$

$$f^E_{\tau_s}(t) = \frac{1}{e^{2t}(1-e^{-T_c})}\big[u(t)-u(t-\frac{T_c}{2})\big], \quad (9)$$

are considered in Fig 2, where $u(\cdot)$ represents the unit step function. Denoting $f_{\Delta\tau}(t)$ as the distribution of $\Delta\tau$ (7), Fig.2 shows that the distribution of the code phase jitter $f_{\Delta\tau}(t)$ has a triangular shape for both $f^U_{\tau_s}(t)$ and $f^E_{\tau_s}(t)$ with the support $|\Delta\tau| \le \tilde{\tau}$. Field observations of multipath delays show that the likelihood of $\tau_{s_l}(t)$ decays in proportion to $1/\tau^2_{s_l}(t)$, which is similar to the exponential distribution $f^E_{\tau_s}$ for a small $\tau_{s_l}(t)$. Moreover, the code phases $\tau_{s_l}(t)$'s are within half of a chip for GPS satellites with an elevation angle $E \ge 30^\circ$ in urban environments [15]. In addition, [15] shows that $f_{\tau_s}(t)$ has a narrower distribution at higher elevation angles. Exploiting the observations in [15], $\tilde{\tau}$ decreases inversely with elevation angle E as

$$\tilde{\tau}(E) \propto E^{-1}, \text{ for } 30^\circ \le E < 90^\circ \text{ and } \tilde{\tau}(30^\circ) = \frac{T_c}{2}. \quad (10)$$

Using (10) and from the observation in [15], for rich multipath environments, we can assume that the distribution of $\Delta\tau$ is

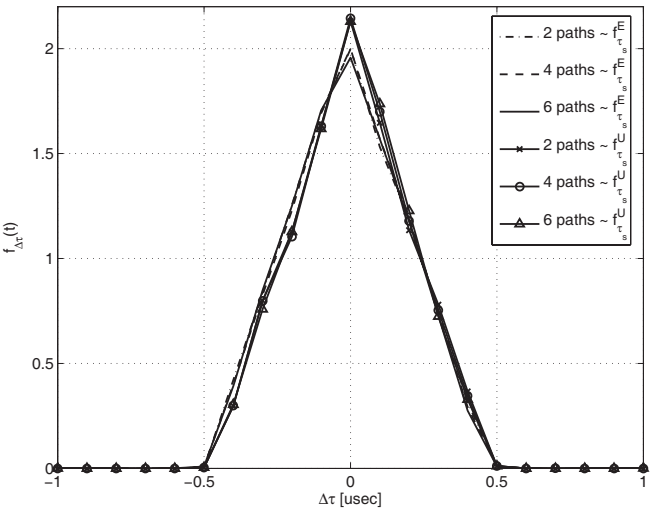

Fig. 2. Statistical distributions of $\Delta\tau$.

expressed as

$$f_{\Delta\tau|E}(t) \simeq \begin{cases} \dfrac{1}{\tilde{\tau}(E)}\Big[1-\dfrac{|t|}{\tilde{\tau}(E)}\Big], & |t|<\tilde{\tau}(E), \\ 0, & \text{otherwise,} \end{cases} \quad (11)$$

for $E \ge 30^\circ$.

Denoting $D_k = 1+V_k/c$, $f_{L1,k} = f_{L1}D_k$, $T_k = \tau_i+(V_k/c)t_i+\tau_m(t_i)$, and $\zeta_k(t) = b_k(t)c_k(t)$, the kth GPS signal arriving at a receiver can be expressed as

$$\begin{aligned} r_k(t) &= \alpha_k(t)s_k(t-\tau(t))+n_k(t) \\ &= \sqrt{2}\alpha_k(t)\zeta_k(D_kt-T_k)\cos(2\pi f_{L1}t+\phi_{r,k}) \\ &\quad +n_k(t), \end{aligned} \quad (12)$$

where $\alpha_k(t)$, $\phi_{r,k}$, and $n_k(t)$ represent the effective fading process of the resolved path, the unknown carrier phase of the received signal, and the noise process with one-sided spectral density N_0, respectively. The fading process $\alpha_k(t)$ has a Rayleigh distribution with a probability density function (PDF) [14]

$$f_{\alpha_k}(\alpha) = \frac{2\alpha}{\Omega}\exp\Big(-\frac{\alpha^2}{\Omega}\Big), \quad (13)$$

where $\Omega = E[\alpha_k(t)^2]$. In-phase and quadrature-phase intermediate frequency (IF) signal components of $r_k(t)$ (12) are obtained by down-converting to the IF band and then band-pass filtering the received signal around the IF frequency, f_{IF}. The frequency down-conversion is accomplished by multiplying by received signal with $\sqrt{2}\cos(2\pi(f_{L1}-f_{IF})t_R)$ and $\sqrt{2}\sin(2\pi(f_{L1}-f_{IF})t_R)$, where

$$t_R = (1+v)t+\delta t \quad (14)$$

is the time measured by the receiver's slightly inaccurate clock with drift rate v and unknown offset δt. Note that we assume v is constant for the time duration of interest. Therefore,

$$\begin{aligned} r^I_{IF,k}(t) &= \alpha_k(t)\zeta_k(D_kt-T_k)\cos(2\pi f_{IF,k}t+\phi_{IF,k}) \\ &\quad +n^I_{IF,k}(t), \end{aligned} \quad (15)$$

$$\begin{aligned} r^Q_{IF,k}(t) &= \alpha_k(t)\zeta_k(D_kt-T_k)\sin(2\pi f_{IF,k}t+\phi_{IF,k}) \\ &\quad +n^Q_{IF,k}(t), \end{aligned} \quad (16)$$

where

$$f_{IF,k} = f_{IF} + \frac{V_k}{c} f_{L1} - v(f_{L1} - f_{IF}), \tag{17}$$

$\phi_{IF,k}$ is an unknown random phase uniformly distributed over $(0, 2\pi]$, and $n^I_{IF,k}(t)$ and $n^Q_{IF,k}(t)$ are in-phase and quadrature-phase noise components, respectively. In many A-GPS applications, the IF signals, $r^I_{IF,k}(t)$ and $r^Q_{IF,k}(t)$, are sampled with the receiver's own clock and stored in a temporary memory for an off-line two-dimensional GPS signal search. The two-dimensional GPS signal search is performed in such a way that all of the code phase hypotheses are tested for each frequency hypothesis. When the frequency hypothesis $\hat{f}_{IF,k}$ being tested is the closest to the IF signal frequency, $f_{IF,k}$, the IF signals, $r^I_{IF,k}(t)$ and $r^Q_{IF,k}(t)$, are multiplied by $2\cos(2\pi\hat{f}_{IF,k}t)$ and $2\sin(2\pi\hat{f}_{IF,k}t)$, respectively, and are low-pass filtered. The resulting baseband signal can be expressed as

$$\begin{aligned} r^I_k(t) &= \alpha_k(t)\zeta_k(D_k t - T_k)\cos(2\pi\delta f_k t + \phi_k) \\ &\quad + n^I_k(t), \end{aligned} \tag{18}$$

$$\begin{aligned} r^Q_k(t) &= \alpha_k(t)\zeta_k(D_k t - T_k)\sin(2\pi\delta f_k t + \phi_k) \\ &\quad + n^Q_k(t), \end{aligned} \tag{19}$$

where $\delta f_k = f_{IF,k} - \hat{f}_{IF,k}$ is smaller than or equal to half of the frequency search step Δf, i.e., $|\delta f_k| \le \Delta f/2$, and $n^I_k(t)$ and $n^Q_k(t)$ are in-phase and quadrature-phase noise components with one-sided spectral density $N_0/2$, respectively. For a given frequency hypothesis, the A-GPS receiver tries to search all possible code phases within a window of time uncertainty given by the cellular network. In an asynchronous cellular network, we assume that the time uncertainty is large, which results in the maximum search window size (1023 chips). Also, we can assume that the bit synchronization is achieved in advance by the techniques in [10] and [11]; therefore, the M chip integration can be as long as the navigation bit duration, 20ms, so that $\zeta_k(D_k t - T_k)$ terms in (18) and (19) can be simplified to $c_k(D_k t - T_k)$. We further assume the satellite Doppler frequency estimate provided by the nearest base station to be very accurate, as the distance between the base station and the A-GPS receiver is negligibly small compared to the distance between the satellite and the A-GPS receiver. Therefore, the locally generated code sequence by the receiver for correlation with the baseband signals, $r^I_k(t)$ and $r^Q_k(t)$, can be expressed as $c_k(D_k t_R - \lambda_i)$, where λ_i is the code phase hypothesis being tested in the ith non-coherent MF. Note that we consider the code phase search step

$$\Delta\lambda = \lambda_i - \lambda_{i-1} = \frac{1}{2}\text{chip} \tag{20}$$

in Fig.1 as a general case.

III. Proposed Decision Variable for A-GNSS in Asynchronous Cellular Networks

Assuming that navigation bit synchronization is achieved, the output of the ith integration from $t = jMT_c$ to $t = (j+1)MT_c$ can be expressed as

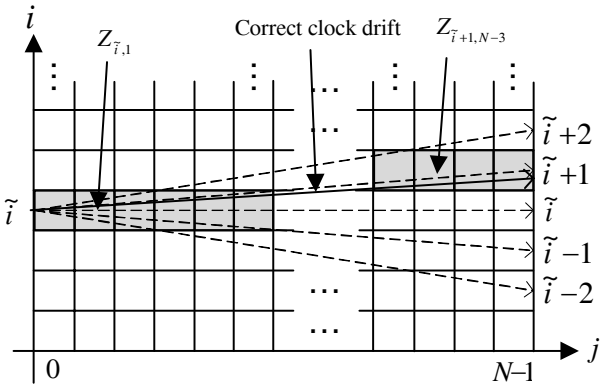

Fig. 3. Clock drift rate hypothesis testing.

$$\begin{aligned} Z_{i,j} &= (Z^I_{i,j})^2 + (Z^Q_{i,j})^2 \\ &= \left[\int_{jMT_c}^{(j+1)MT_c} r^I_k(t)c_k(D_k t_R - \lambda_i)\,dt\right]^2 \\ &\quad + \left[\int_{jMT_c}^{(j+1)MT_c} r^Q_k(t)c_k(D_k t_R - \lambda_i)\,dt\right]^2, \end{aligned} \tag{21}$$

where $M = 20460$ is the total number of PRN chips in 20ms and λ_i is the ith examined code phase. Due to the unknown clock drift rate v, $Z_{i,j}$ can vary as j increases from $j = 0$ to $N-1$. For example, if we assume that λ_i is the correct code phase at $j = 0$ and ignore the effect of the code phase jitter, $Z_{i,N-1} = Z_{i,0}R^2(0.5\mu s) \simeq Z_{i,0}/4$ when $v = 0.2\mu s$ per second and $N = 125$. In practice, the maximum possible value of v is limited by the frequency tolerance requirements of the asynchronous cellular networks and mobile terminals [7]-[9]. Therefore, there may be a limited number of clock drift rate hypotheses to test when all of the MF outputs $Z_{i,j}$ ($i = 0, 1, 2, ...N_I - 1$, and $j = 0, 1, 2, ...N-1$) are obtained. Fig.3 illustrates an example of the clock drift rate hypothesis testing, where 5 clock drift rate hypotheses (depicted by the 5 arrows starting from the point at $(i = \tilde{i}, j = 0)$) are being tested. The shaded bin at the jth M-chip integration in Fig.3 is the closest code phase hypothesis to the correct code phase.

Denoting $v_{max} (= 0.2\mu s$ per second for GSM and WCDMA) as the maximum possible value of v and $\delta v = \Delta\lambda/(NMT_c)$ as the search step size between adjacent clock drift rate hypotheses, there are $N_v = 1 + 2\lceil v_{max}/\delta v \rceil$ clock drift rate hypotheses to test, where $\lceil\cdot\rceil$ represents an arithmetic roundup function. Note that the clock drift rate hypothesis testing requires only arithmetic summations of the integrator outputs, $Z_{i,j}$. For a hypothesis $v = k\delta v$, we can use a decision variable using a single H_1 cell for code phase and clock drift rate hypotheses testing. That is written as

$$Z_S = Z|H_1 = \sum_{j=0}^{N-1} Z_{(i+\lfloor \frac{jk\Delta\lambda}{N} \rceil) mod N_I, j}, \tag{22}$$

where i is the index of a code phase λ_i at the beginning of the hypothesis testing ($j = 0$), k is an integer such that $|k| \le (N_v - 1)/2$, $\lfloor\cdot\rceil$ represents rounding to the nearest integer, and $x \ mod \ N_I$ denotes the x modulo N_I operation. In the parallel search, Z_S (22) is computed for all possible pairs of

code phase and clock drift rate hypotheses, and the pair with the largest value of Z_S is accepted. Note that a conventional decision variable using a single H_1 cell can be written as

$$Z_C = \sum_{j=0}^{N-1} Z_{i,j}, \tag{23}$$

which neglects the possible non-zero clock drift rate. By using Z_S (22) instead of Z_C (23), we can expect an increment in the complexity due to the clock drift rate hypothesis testing. However, the common major load in computing Z_S and Z_C is the M-chip integration for $Z_{i,j}$ (21); thus, the complexity increment of the single H_1-cell hypothesis testing over the conventional case is negligible.

In general, the effect of the clock drift rate on the decision variable, such as Z_S (22), can be modeled by the distribution of the accumulated clock drift Δt during each M-chip integration. Without loss of generality, we can assume that the accumulated clock drift is uniformly distributed. Therefore,

$$f_{\Delta t}(t) \simeq \begin{cases} \tilde{t}^{-1}, & |t| \le \tilde{t}, \\ 0, & \text{otherwise}, \end{cases} \tag{24}$$

where $\tilde{t} = \Delta\lambda/(2N)$ because, with the decision variable (22), we can find the code phase of the resolved path within $\pm\Delta\lambda/2$ from the correct code phase at the end of the search process over dwell time NMT_c. For a $\Delta\lambda \le \frac{1}{2}$chip, the clock drift may not result in a potential sensitivity loss in the acquisition process. However, when there is a large time-varying code phase jitter $\Delta\tau$ (7) with distribution $f_{\Delta\tau|E}(t)$ (11) due to short-delay multipaths, the decision variables (22) and (23) may have a considerable sensitivity loss.

One means of improving GPS sensitivity, when there exists a non-negligible code phase jitter $\Delta\tau$ in the resolved path and a nonzero clock drift rate in the receiver clock, is to use two adjacent H_1 cells of the resolved path. In [16], it is discussed that, in a conventional spread spectrum code phase search with a half chip step size, there exist two adjacent H_1 cells which are expected to be at $\pm\frac{1}{4}$ chip from the correct code phase; in this case, the sensitivity is improved using two adjacent H_1 cells jointly in the code phase hypothesis testing. Intuitively, the joint two H_1 cells hypothesis testing may improve robustness to the varying code phase jitter $\Delta\tau$ and unknown clock drift rate. Therefore, we propose a decision variable using the two adjacent H_1 cells jointly in the presence of short-delay multipaths for A-GPS in asynchronous cellular networks:

$$\begin{aligned} Z_D &= Z|(H_1, H_1) \\ &= \sum_{h=0}^{1} \sum_{j=0}^{N-1} Z_{(i+\lfloor \frac{jk\Delta\lambda}{N} \rceil + h) mod N_I, j}. \end{aligned} \tag{25}$$

As in the Z_S case (22), the complexity increment in computing Z_D (25) over Z_C (23) is negligible.

IV. Statistics of the Proposed Decision Variables

As briefly discussed in the beginning of Section II, t_R can drift by $\pm 0.2\mu s$ per second. Therefore, we assume that the clock drift during each MT_c second ($20ms$) integration is negligible. In addition, we assume that the code phase measurement error $\tau_m(t)$ (6) varies slowly enough that $\tau_m(t) = \tau_{m,j}$ for $t \in [jMT_c, (j+1)MT_c)$ but, at the same time, it varies fast enough that $\tau_{m,j}$ and $\tau_{m,l}$, $j \neq l$, are independent. Under this assumption, $\Delta\tau_j = \tau_{m,j+1} - \tau_{m,j}$ is a sequence of independent random variables, whose distribution is given in (11). Finally, we assume that the fading coefficient $\alpha_k(t)$ varies slowly enough that it remains constant for $t \in [jMT_c, (j+1)MT_c)$ but fast enough that it varies independently between two successive integrations. We let $\alpha_{i,j}$ be the fading coefficient at the ith integrator output for the interval $[jMT_c, (j+1)MT_c)$. Hence, according to this assumption, $\alpha_{i,j}$ and $\alpha_{i,l}$, $j \neq l$, are independent.

From the above assumptions, the statistics of in-phase and quadrature-phase components, $Z^I_{i,j}$ and $Z^Q_{i,j}$ (21), of a H_1 cell can be expressed as

$$E[Z^I_{i,j}|H_1] = A_1(\nu|E) MT_c \alpha_{i,j} \cos(\phi_k), \tag{26}$$

$$E[Z^Q_{i,j}|H_1] = A_1(\nu|E) MT_c \alpha_{i,j} \sin(\phi_k), \tag{27}$$

and

$$Var[Z_{I_{i,j}}|H_1] = A_2(\nu|E)(MT_c\alpha_{i,j}\cos(\phi_k))^2 + V_0, \tag{28}$$

$$Var[Z_{Q_{i,j}}|H_1] = A_2(\nu|E)(MT_c\alpha_{i,j}\sin(\phi_k))^2 + V_0, \tag{29}$$

where

$$A_1(\nu|E) = \int_{-\infty}^{\infty} R(t+\nu)\left[f_{\Delta\tau|E}(t) * f_{\Delta t}(t)\right] dt, \tag{30}$$

$$\begin{aligned} A_2(\nu|E) = &\int_{-\infty}^{\infty} R^2(t+\nu)\left[f_{\Delta\tau|E}(t) * f_{\Delta t}(t)\right] dt \\ &- A_1^2(\nu|E), \end{aligned} \tag{31}$$

$$V_0 = \frac{1}{2} MT_c N_0.$$

Here, in the equations above (from (26) to (31)), $\nu \in [-T_c/4, T_c/4)$ for single H_1 cell hypothesis testing, $\nu \in [0, T_c/2)$ for the early H_1 cell and $\nu \in [0, T_c/2)$ for the late H_1 cell of joint two H_1 cells hypothesis testing. For an A-GPS receiver in a synchronous cellular network, the clock drift rate is negligibly small. Thus, it can be assumed that $f_{\Delta t}(t) = \delta(t)$ in (30) and (31). On the other hand, without clock drift rate hypothesis testing in an asynchronous cellular network, $\tilde{t}$ in (24) can be much larger than $\Delta\lambda/(2N)$, implying that A_1 in (30) can become very small. Fig. 4 shows numerical evaluations of $A_1(\nu|E)$ (30) with respect to $\nu \ge 0$[1] for $E = 30°$. Clearly, A_1 decreases as $\tilde{\tau}$ or $\tilde{t}$ increases. Note that the average value of $A_1(\nu|E)$ for the single H_1 cell and joint two H_1 cells hypothesis testings can be expressed as

$$\bar{A}_1^S(E) = \frac{2}{T_c} \int_{-T_c/4}^{T_c/4} A_1(\nu|E)\, d\nu, \tag{32}$$

$$\bar{A}_1^D(E) = \frac{2}{T_c} \int_{0}^{T_c/2} A_1(\nu|E)\, d\nu, \tag{33}$$

respectively, given that ν is uniformly distributed. In addition, due to the symmetry of $A_1(\nu|E)$, (33) covers both the early and the late H_1 cells of the joint two H_1-cells hypothesis

[1]Given that $R(t)$, $f_{\Delta\tau|E}(t)$, and $f_{\Delta t}(t)$ are all symmetric about the y-axis, $A_1(\nu|E)$ is also symmetric about the y-axis.

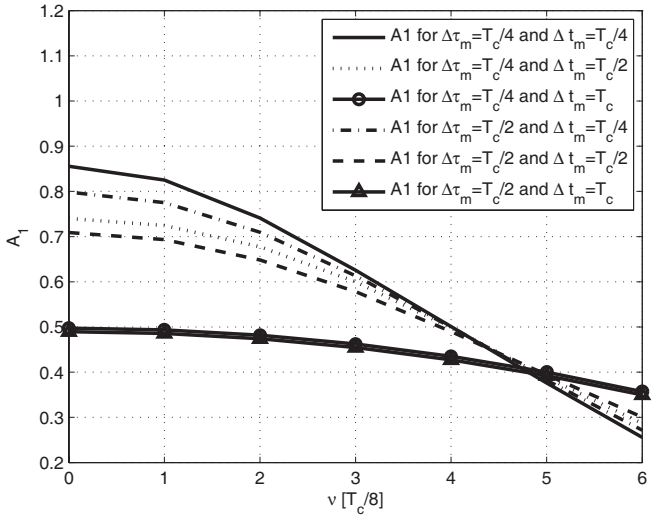

Fig. 4. Numerical evaluations of A_1. ($E = 30°$).

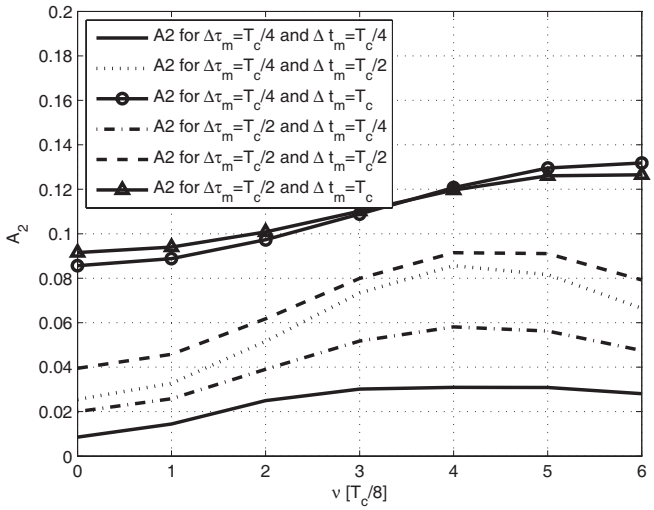

Fig. 5. Numerical evaluations of A_2. ($E = 30°$).

testing. The numerical evaluations in Fig.4 show that $\bar{A}_1^S(E) \simeq 0.807$ and 0.684 when $(\tilde{\tau}, \tilde{t}) = (T_c/4, T_c/4)$ and $(\tilde{\tau}, \tilde{t}) = (T_c/2, T_c/2)$, respectively. Similarly, $\bar{A}_1^D(E) \simeq 0.710$ and 0.624 when $(\tilde{\tau}, \tilde{t}) = (T_c/4, T_c/4)$ and $(\tilde{\tau}, \tilde{t}) = (T_c/2, T_c/2)$, respectively. Note that the ratio of $\bar{A}_1^S(E)$ (32) to $\bar{A}_1^D(E)$ (33) decreases to 1 as $\tilde{\tau}$ and $\tilde{t}$ increase. For example, when $\tilde{t} = T_c$, $\bar{A}_1^S(E)$ (32) is approximately identical to $\bar{A}_1^D(E)$ (33), as shown in Fig. 4.

Fig. 5 shows numerical evaluations of $A_2(\nu|E)$ (31). From Fig. 4 and Fig. 5, we can conclude that $A_2(\nu|E)$ is negligibly small compared to $A_1(\nu|E)^2$ when $|\nu| \leq 3T_c/8$ and $\tilde{t} < T_c/2$. In other words, in the case of large $|\nu|$ and large $\tilde{t}$ values, $A_2(\nu|E)$ is not negligible compared to $A_1(\nu|E)^2$. Based on the observations in Fig. 4 and Fig. 5, the second terms in (28) and (29) can be neglected for low carrier-to-noise-density ratios (C/N_0) and $\tilde{t} \leq T_c/2$; thus, (28) and (29) are simplified as

$$Var[Z_{i,j}^I|H_1] = Var[Z_{i,j}^Q|H_1] \simeq V_0. \tag{34}$$

Note that when H_0 cells are being tested instead of H_1 cells, the expected values in (26) and (27) become zero.

V. Performance Analysis

A. Algebraic analysis

One useful means of evaluating the acquisition performance of a decision variable is to find the receiver operating characteristics (ROC) [17]. In this section, we compare the ROCs of the proposed decision variables Z_D (25) and Z_S (22) using the statistics obtained in Section IV. For the single H_1 cell hypothesis testing with Z_S (22), the probability distribution P_0 when the signal is not present and the probability distribution P_1 when the signal is present are expressed as [17]

$$P_0(Z_s) = \frac{1}{2V_0} \exp[-Z_s/(2V_0)], \tag{35}$$

$$P_1(Z_s) = \frac{1}{V_F^S(\nu|E)} \exp[-Z_s/V_F^S(E)], \tag{36}$$

where

$$V_F^S(E) = 2V_0 + \bar{A}_1^S(E)^2 \Omega M^2 T_c^2. \tag{37}$$

As Z_S (22) is composed of $N(\gg 1)$ independent exponential observations, the false alarm probability and the detection probability for the single H_1 cell hypothesis testing with a detection threshold γ_1 can be expressed as [17]

$$P_F^S(\gamma_1) = \exp[-\gamma_1/(2V_0)] \sum_{k=0}^{N-1} \frac{(\gamma_1/(2V_0))^k}{k!}, \tag{38}$$

$$P_D^S(\gamma_1) = \exp[-\gamma_1/V_F(\hat{\nu}|E)] \sum_{k=0}^{N-1} \frac{(\gamma_1/V_F(\hat{\nu}|E))^k}{k!}. \tag{39}$$

For the joint two H_1-cells hypothesis testing, as Z_D (25) is composed of $2N$ observations, the false alarm probability is computed similarly to (38), as

$$P_F^D(\gamma_1) = \exp[-\gamma_1/(2V_0)] \sum_{k=0}^{2N-1} \frac{(\gamma_1/(2V_0))^k}{k!}. \tag{40}$$

At this point, to derive the detection probability of the joint two H_1-cells hypothesis testing, we first derive the PDF of Z_D (25) when the signal is present. Let us consider two different exponential distributions,

$$f_a(z) = a \exp(-az), \tag{41}$$

$$f_b(z) = b \exp(-bz), \tag{42}$$

which correspond to the distributions of the early and the late H_1 cells, respectively. We define Z_D as the sum of $2N$ independent random variables, where N of them are distributed by $f_a(z)$ and the others are distributed by $f_b(z)$. Thus, the PDF of Z_D, $P_1(Z_D)$, can be found using the moment generating function method [14]. The Laplace transform of the probability $P_1(Z_D)$ can be expressed as

$$\mathcal{L}\{P_1(Z_D)\} = \frac{a^N b^N}{(s+a)^N (s+b)^N}. \tag{43}$$

The inverse Laplace transform of (43) can be readily found in [18] as

$$P_1(Z_D) = \frac{\sqrt{\pi} a^N b^N}{\Gamma(N)} \Big(\frac{Z_D}{a-b}\Big)^{N-\frac{1}{2}} \cdot \exp\Big(-\frac{a+b}{2} Z_D\Big) I_{N-\frac{1}{2}}\Big(\frac{a-b}{2} Z\Big), \tag{44}$$

where $\Gamma(\cdot)$ is the Gamma function such that

$$\Gamma(x) = \int_0^\infty t^{x-1} e^{-t}\, dt, \tag{45}$$

and $I_{N-\frac{1}{2}}(\cdot)$ is the modified Bessel function of an order equal to $N-\frac{1}{2}$. Assuming that C/N_0 of the GPS signal is very low and that N is very large, we have $0 < \frac{a-b}{2} Z \ll \sqrt{N+\frac{1}{2}}$. Therefore, the last term in (44) can be approximated as [18]

$$I_{N-\frac{1}{2}}\left(\frac{a-b}{2} Z\right) \simeq \frac{2^{2N-1}\Gamma(N)}{\sqrt{\pi}\Gamma(2N)} \left(\frac{a-b}{4} Z\right)^{N-\frac{1}{2}}. \tag{46}$$

In addition, we assume $a \approx b$, which is reasonable when C/N_0 is very low or when the two adjacent H_1 cells are located nearly the same distance from the resolved path correlation peak or when the integrator output of the resolved path has a round or flat top due to the multipath channel. This gives

$$\frac{a+b}{2} \simeq \sqrt{ab}. \tag{47}$$

Using (46) and (47), $P_1(Z)$ (44) can be approximated as

$$P_1(Z_D) \simeq \left(\frac{a+b}{2}\right)^{2N} \frac{Z_D^{2N-1}}{\Gamma(2N)} \exp\left(-\frac{a+b}{2} Z_D\right). \tag{48}$$

From (48), a generalized form of the detection probability for the joint two H_1-cells hypothesis testing with a detection threshold γ_1 can be found as

$$P_D^D(\gamma_1) \simeq \exp\left(-\frac{a+b}{2}\gamma_1\right) \sum_{k=0}^{2N-1} \frac{(a+b)^k \gamma_1^k}{2^k k!}. \tag{49}$$

Here, let us consider how to determine the parameters a and b in (49). For the joint two H_1-cells hypothesis testing, the statistical dependency of the fading coefficients $\alpha_{i,j}$'s between the two adjacent H_1 cells is an important factor that affects the performance. The distribution of the fading coefficient is closely related to the statistics of the multipath channel. Fig. 6 illustrates this relationship for simple single and two-path channels. When the channel has only one path or when the delay spread of multiple paths are very small compared to the chip duration, the fading coefficient of the two adjacent H_1 cells can be highly correlated since there appears a single undistorted peak, as shown in Fig. 6 (a). On the other hand, when the channel paths are sufficiently far apart as in 6 (b), the fading coefficients of the two adjacent H_1 cells cannot be identical; rather, they can be assumed to be almost independent. In fact, since the fading coefficients depend on the multipath channel distribution, they are also correlated to the code phase jitter $\Delta\tau$. However, the exact joint distribution of the fading coefficient and the code phase jitter cannot be derived immediately; thus, we consider their effects on the performance separately.

First, we assume that the fading coefficients of the two adjacent H_1 cells are equal, which corresponds to the case shown in Fig. 6 (a). Equivalently, we can consider this as a case in which only one on the two added cells in Z_D (25) has a signal with twice the power and the other cell has no signal.

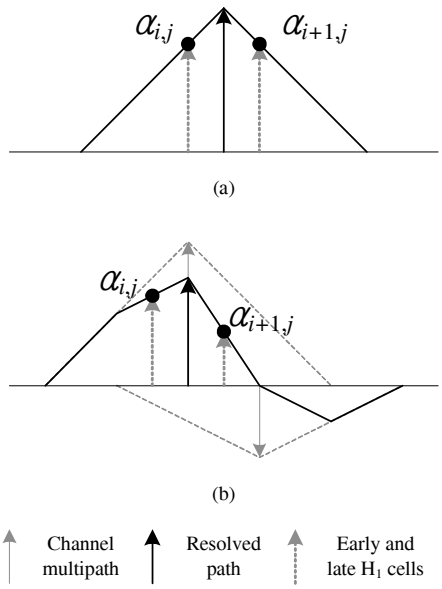

Fig. 6. Fading coefficient at the integrator output. (a) Single path channel model. (b) Two path channel model with $T_c/2$ delay between paths.

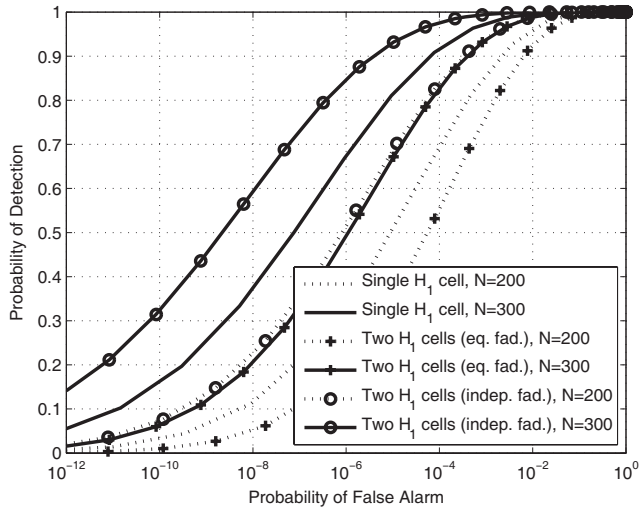

Fig. 7. ROC when $\Delta\tau_m = T_c/4$ and $\Delta t_m = T_c/4$. ($C/N_0 = 36$dB·Hz, 4MHz noise bandwidth, $E = 30°$).

Therefore, we can use the following set of parameters:

$$a = \frac{1}{2V_0 + 2\bar{A}_1^D(E)^2 \Omega M^2 T_c^2}, \tag{50}$$

$$b = \frac{1}{2V_0}. \tag{51}$$

In the opposite case in which the fading coefficients of the two adjacent H_1 cells are statistically independent, the following set of parameters can be used:

$$a = b = \frac{1}{2V_0 + \bar{A}_1^D(E)^2 \Omega M^2 T_c^2}. \tag{52}$$

Figure 7 shows the ROC of Z_D (25) and that of Z_S (22) to compare the statistical average performance when the code phase jitter and clock drift rate are small (when $(\tilde{\tau}, \tilde{t}) = (T_c/4, T_c/4)$, $C/N_0 = 36$dB·Hz with a noise bandwidth of 4MHz, and $E = 30°$). Fig.8 shows the ROC when the code phase jitter and clock drift rate are not small

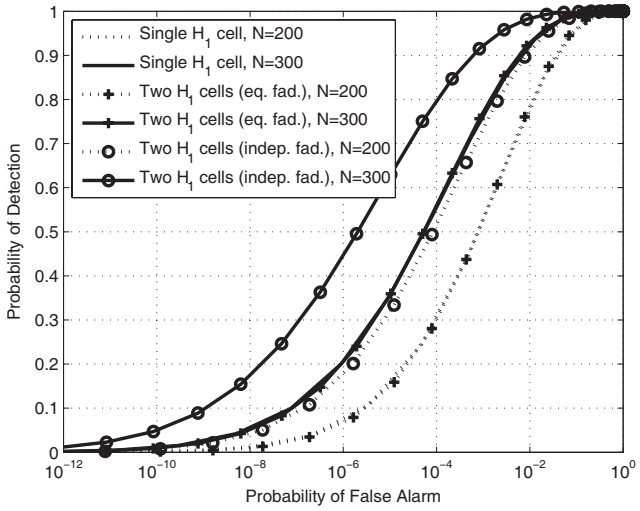

Fig. 8. ROC when $\Delta\tau_m = T_c/2$ and $\Delta t_m = T_c/2$. ($C/N_0 = 36$dB·Hz, 4MHz noise bandwidth, $E = 30°$).

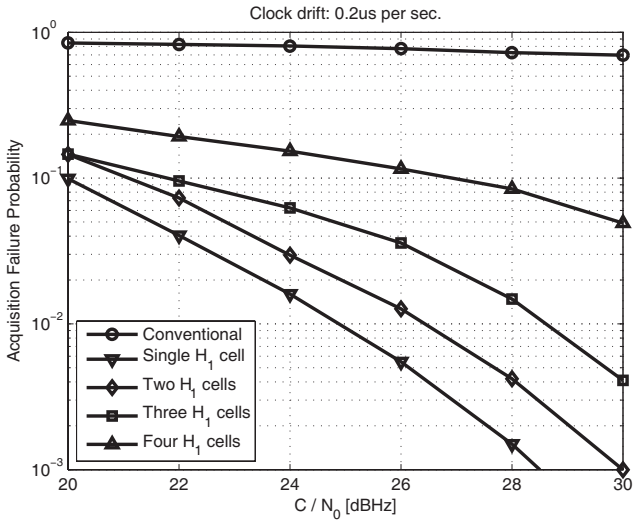

Fig. 9. Acquisition failure probability for $1/4$chip path delay.

(when $(\tilde{\tau}, \tilde{t}) = (T_c/2, T_c/2)$, $C/N_0 = 36$dB·Hz with a noise bandwidth of 4MHz, and $E = 30°$). Figs. 7 and 8 demonstrate that the joint two H_1-cells hypothesis testing outperforms the single H_1-cell hypothesis testing when the fading coefficients of the two adjacent H_1 cells are independent. This is an expected result since, theoretically, the ROC of the joint two H_1 cells with N non-coherent accumulation can be as good as that of a single H_1 cell with $2N$ non-coherent accumulation, when $\bar{A}_1^S(E)$ (32) is identical to $\bar{A}_1^D(E)$ (33). However, when the fading coefficients of the two adjacent H_1 cells are equal, the performance of the joint two H_1-cells hypothesis testing can be worse than that of the single H_1-cell hypothesis testing.

B. Numerical analysis

In this subsection, we perform a Monte Carlo simulation for the performance comparison between the single H_1-cell and the joint two H_1-cells hypothesis testings. As a baseline, we also consider a conventional single H_1-cell hypothesis testing without a clock drift rate hypothesis testing. In addition, we also include more than two H_1-cells hypothesis testings,

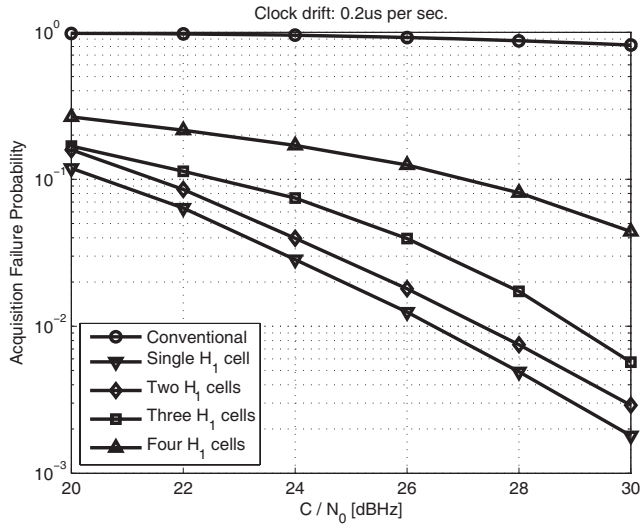

Fig. 10. Acquisition failure probability for $1/3$chip path delay.

including the joint three and the joint four H_1-cells hypothesis testings, in the numerical analysis. As discussed in [13], there can be more than two H_1 cells when the channel is severely dispersive. In such a situation, joint three or four H_1-cells hypothesis testings can outperform the single or the joint two H_1-cells hypothesis testings. Thus, we evaluate their performances and compare them with other schemes.

As a performance measure, we use the acquisition failure probability, i.e., the probability that the hypothesis with the maximum decision variable is not correct, which is within $T_c/2$ from the code phase of the true resolved path. In the simulation, we use common GPS C/A code parameters. For the other parameters, we assume $E = 30°$, $\Delta\lambda = \frac{T_c}{2}$, a C/N_0 range from 20dB·Hz to 30dB·Hz, and a 4MHz noise bandwidth. We also consider a 4s dwell time with 20ms integrations for the hypothesis testing, and, thus, $N_I = 2046$ and $N = 200$. Finally, we assume that the clock drift rate is 0.2μs per second and that the number of clock drift rate hypotheses N_v for each code phase hypothesis is 5.

As the channel model, we assume a multipath channel consisting of two paths with independent and identical fading distribution, as in Fig. 6 (b). We adjust the delay between the two paths to observe the effect of channel dispersion on the performance. Fig. 9 shows the acquisition failure probabilities of various schemes for different C/N_0 values when the delay between two channel paths is $T_c/4$. With this relatively small delay, the fading coefficients of the two adjacent H_1 cells are highly correlated. Thus, as expected in the analysis of Section V-A, the proposed joint two H_1-cells hypothesis testing performs worse than the proposed single H_1-cell hypothesis testing. Likewise, the joint three and four H_1-cells hypothesis testings perform even worse. Note that the baseline performance is considerably worse than the others. This occurs because the baseline assumes that the code phase is fixed at a point while it can drift by almost T_c in the dwell time. Therefore, it is highly improbable that the code phase detected by the baseline remains within $T_c/2$ to the true code phase of the resolved path during the dwell time.

Figures 10 and 11 depict the acquisition failure probabilities

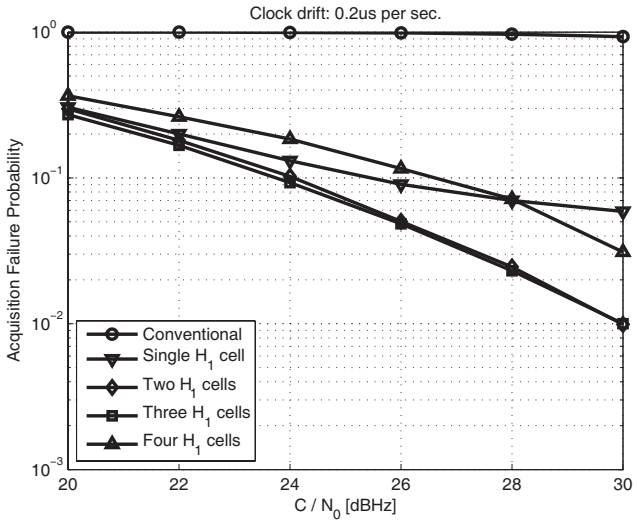

Fig. 11. Acquisition failure probability for $1/2$chip path delay.

for $T_c/3$ and $T_c/2$ delays between channel paths, respectively. As the channel dispersion increases, the overall performances tend to degrade. However, the speed of the deterioration differs depending on the scheme. In particular, the performance of the single H_1-cell hypothesis testing degrades most rapidly, while the joint four H_1-cells hypothesis testing is most robust. For the channel path delay $T_c/2$, the performances of the joint two and three H_1-cells hypothesis testings are almost equal, topping the performance of the single H_1-cell hypothesis testing. Thus, we conclude that, within the practical range of channel dispersion for the GPS C/A signal, which is below $T_c/2$ as observed in [15], the joint two H_1-cells hypothesis testing is the best choice, since it generally performs well and is robust to changes in the channel dispersion.

VI. Conclusion

In this paper, two dominant causes of A-GNSS sensitivity loss in asynchronous cellular networks were investigated: Code phase jitters in rich multipath environments, such as dense urban canyons, and unknown non-zero clock drift rate due to the non-negligible frequency and timing uncertainties in the downlink of the asynchronous cellular signal. An A-GNSS sensitivity improvement scheme using two adjacent H_1 cells for code phase hypothesis testing and clock drift rate hypothesis testing was suggested. It was analytically demonstrated that the A-GNSS sensitivity can be improved for a given length of non-coherent accumulations. Through numerical simulation, it was also shown that the joint two H_1-cells hypothesis testing outperforms the conventional scheme in terms of acquisition performance. Moreover, it is robust to changes in the channel dispersion in a practical range under half the chip duration.

References

[1] TIA/EIA IS-801-1, Position determination service standards for dual-mode spread spectrum systems-addendum, Mar. 2001.
[2] 3GPP TS 25.305, Stage 2 functional specification of UE positioning in UTRAN, V4.7.0, Dec. 2003.
[3] E. Souour and S. C. Gupta, "Direct-sequence spread-spectrum parallel acquisition in a fading mobile channel," *IEEE Trans. Commun.*, vol. 38, no. 7, pp. 992-998, July 1990.
[4] I. F. Progri, W. R. Michalson, J. Wang, and M. C. Bromberg, "Indoor geolocation using FCDMA pseudolites: signal structure and performance analysis," *Navigation J. Inst. Nav.*, vol. 54, no. 3, pp. 242-256, Fall 2007.
[5] P. Misra and P. Enge, *Global Positioning System: Signals, Measurements, and Performance*, 2nd edition. Ganga-Jamuna Press, 2006.
[6] E. D. Kaplan and C. J. Hegarty, *Understanding GPS: Principles and Applications*, 2nd edition. Artech House, 2006.
[7] 3GPP TS 45.010, "Radio subsystem synchronization (Release 8)," V8.0.0, May 2008.
[8] 3GPP TS 25.104, "Base Station (BS) radio transmission and reception (FDD) (Release 8)," V8.0.0, Sep. 2007.
[9] 3GPP TS 25.101, "User Equipment (UE) radio transmission and reception (FDD) (Release 8)," V8.0.0, Sep. 2007.
[10] M.-Y. Chung and K.-T. Feng, "Adaptive GPS acquisition technique in weak signal environment," in *Proc. IEEE 63rd VTC, 2006-Spring*, pp. 2612-2616, vol. 6, May 2006.
[11] C. Yang, T. Nguyen, E. Blasch, and M. Miller, "Post-correlation semi-coherent integration for high-dynamic and weak GPS signal acquisition," in *Proc. IEEE/ION Position, Location, and Navigation Symposium*, pp. 1341-1349, May 2008.
[12] I. F. Progri, M. C. Bromberg, and J. Wang, "Markov chain, Monte Carlo global search and integration for Bayesian, GPS, parameter estimation," *Navigation J. Inst. Nav.*, vol. 56, no. 3, pp. 195-204, Fall 2009.
[13] L.-L. Yang and L. Hanzo, "Serial acquisition performance of single-carrier and multicarrier DS-CDMA over Nakagami-m fading channels," *IEEE Trans. Wireless Commun.*, vol. 1, no. 4, pp. 692-702, Oct. 2002.
[14] A. Papoulis, *Probability, Random Variables and Stochastic Processes*, 3rd edition. New York: McGraw-Hill, 1991.
[15] A. Steingass and A. Lehner, "Measuring the navigation multipath channel—a statistical analysis," *ION GNSS 2004*, Long Beach, USA, Sep. 2004.
[16] L.-L. Yang and J. Simsa, "Performance evaluation of spread-spectrum code acquisition using four-state Markov process," *IEEE Proc.-Commun.*, vol. 147, no. 4, pp. 231-238, Aug. 2000.
[17] A. J. Viterbi, *CDMA Principles of Spread Spectrum Communication*. Addison Wesley, 1995.
[18] Staff of Research and Education Association, *Handbook of Mathematical, Scientific, and Engineering Formulas, Tables, Functions, Graphs, Transforms*. Research and Education Association, 1992.

Seung-Hyun Kong received a B.S.E.E. from Sogang University, Korea, in 1992, an M.S.E.E. from Polytechnic University, New York, in 1994, and a Ph.D. degree in Aeronautics and Astronautics from Stanford University, CA, in Jan. 2006. From 1997 to 2000, he was a research member of CDMA standard development group and mobile positioning technology team at Samsung Electronics, Inc., Korea. From 2000 to 2004, he worked for Nexpilot Inc., Korea, as an R&D lead for UMTS location system development. He was with Qualcomm, Inc., San Diego, where he was engaged in developing advanced location technologies such as cooperative localization for mobile nodes and urban GPS enhancements from 2007 to 2009. In January 2010, he joined the Division of Aerospace Engineering, Korea Advanced Institute of Science and Technology (KAIST), Daejeon, Rep. of Korea, where he is an Assistant Professor. His research interests include technologies for urban and indoor navigation, statistical analysis of urban multipath channels, and signal acquisition and tracking algorithms.

Wooseok Nam (S'04-M'09) was born in Busan, Republic of Korea, in 1980. He received his B.S., M.S., and Ph.D. degree in the Department of Electrical Engineering at KAIST in 2002, 2004, and 2009, respectively. His research interests include network information theory, adaptive signal processing, and digital modem design.